Mechanical Systems and Signal Processing ∎ (∎∎∎∎) ∎∎∎–∎∎∎

Contents lists available at ScienceDirect

Mechanical Systems and Signal Processing

journal homepage: www.elsevier.com/locate/ymssp

Fault detection in heavy duty wheels by advanced vibration processing techniques and lumped parameter modeling

M. Malago', E. Mucchi *, G. Dalpiaz

Engineering Department, University of Ferrara, Via Saragat, 1 I-44122 Ferrara, Italy

ARTICLE INFO

Article history:
Received 25 February 2013
Received in revised form
24 June 2015
Accepted 27 September 2015

Keywords:
Condition monitoring
Quality control
Heavy duty wheel
Synchronous average
Cyclostationary
Lumped parameter model

ABSTRACT

Heavy duty wheels are used in applications such as automatic vehicles and are mainly composed of a polyurethane tread glued to a cast iron hub. In the manufacturing process, the adhesive application between tread and hub is a critical assembly phase, since it is completely made by an operator and a contamination of the bond area may happen. Furthermore, the presence of rust on the hub surface can contribute to worsen the adherence interface, reducing the operating life. In this scenario, a quality control procedure for fault detection to be used at the end of the manufacturing process has been developed. This procedure is based on vibration processing techniques and takes advantages of the results of a lumped parameter model. Indicators based on cyclostationarity can be considered as key parameters to be adopted in a monitoring test station at the end of the production line due to their not deterministic characteristics.

1. Introduction

Nowadays the identification of faulty components represents a fundamental issue in terms of cost reduction for recall or product replacements. The development of dedicated controls at the end of the production phase, i.e. through a monitoring and diagnostic analysis, can represent a possible approach to reach this target [1,2]. Condition monitoring and fault detection are generally referred to as the evaluation of the state of a system through the selection of measurable parameters, which will change with the state of health of the system. On the other hand, fault diagnosis is a more rigorous action which requires the identification of the component that causes the deviation from the normal state [2–5]. Condition monitoring and diagnostics can be achieved by using different kinds of data as input (e.g. pressure, temperature, torque), nevertheless the vibration analysis can be considered extremely widespread since mechanical faults in machinery often show their presence through abnormal vibration signals. As a consequence, the purpose of condition monitoring is to use information extracted from the system signature in order to detect faults or to define its state of health: a change in the vibration signature not only indicates a change in the system conditions, but also directly points to the source of the signal alteration.

A condition monitoring process based on experimental data is achieved by different steps. Firstly, a relevant number of healthy and faulty components are realized and analyzed in order to detect the most suitable sensor, the optimal position and the operational condition able to emphasize the component changes. The subsequent step consists in the measurement of experimental data. Generally, the acquired signals need to be processed through appropriate techniques in order to

* Corresponding author. Tel.: +39 0532 974911.
E-mail address: emiliano.mucchi@unife.it (E. Mucchi).

http://dx.doi.org/10.1016/j.ymssp.2015.09.043
0888-3270/

Please cite this article as: M. Malago', et al., Fault detection in heavy duty wheels by advanced vibration processing techniques and lumped parameter modeling, Mech. Syst. Signal Process. (2015), http://dx.doi.org/10.1016/j.ymssp.2015.09.043

extract the maximum amount of information. Finally, well suited indicators/coefficients are applied to the processed signal, objectifying the anomaly presences and defining pass–fail reference values.

The Synchronous Averaging (SA) is a rather common method for the early detection of failure in rotational elements such as gears, bearings and wheels and it is basically obtained by synchronizing the samplings of the measured signal with the rotational element of interest and by evaluating the ensemble average over many revolutions [6–8]. Hence, SA contains only the components synchronized with the revolution of the rotational element being studied. If sufficient averages are taken, the SA closely approximates a truly periodic signal with periodicity corresponding to one revolution of the selected rotational element [1,2]. This process strongly reduces the effects of the vibration sources non-synchronous with the reference, including other rotational elements and the background noise. Classically, this has been accomplished using a tachometer signal [9,10].

Particular techniques have also been proposed for angular resampling of the vibration signal without the need of a speed sensor [7,11]. This method is carried out by means of a keyphasor signal that is typically at once per shaft revolution event. Such a signal is used to measure the shaft speed and represents the reference for measuring the vibration phase angle. Normally it is assumed that the rotating component is undergoing constant angular acceleration in order to determine the re-sample times. The corresponding amplitudes are calculated by interpolating between the sampled data using a linear interpolation method. As a result, the SA of the vibration signal allows to attenuate the periodic events not synchronous with the rotating component of interest and to reduce background noise. The resulting signal average is the ensemble average of the angle domain signal, synchronously sampled with respect to the component rotation. The main advantage of SA is to extract its deterministic part from a complex vibration signal, i.e. the events that are repeated periodically with the rotation of interest.

A further advanced tool adopted for investigating the relationships between spectral components is the cyclostationary theory [3,4,10]. More specifically, a signal is cyclostationary if some of its statistics present periodicities. As previously described, averaging can make it possible to extract the deterministic part of the signal. If the signal obtained after subtracting this deterministic part from the synchronized signal does not exhibit cyclostationarity, the signal is said to be cyclostationary at an order "1". In general terms, a signal is cyclostationary at an order "n" if its statistical properties at order "n" are periodic.

The pass/fail thresholds are generally defined starting from the analysis of a large group of healthy components applying statistical techniques with the a-priori knowledge of the real data distribution. However, in case of a small number of samples, it is advisable to use non-statistical techniques. This is the case adopted in this research activity in which Tukey's non-statistical method has been applied to a group of 15 healthy wheels.

The Tukey's method [13] is a simple but effective procedure for the identification of anomalies in a distribution of data. Unlike common statistical procedures, Tukey's method is a non-parametric technique that does not consider any distributional assumptions about the statistical behavior of the data.

Moreover, in order to improve the development/assessment of processing techniques in a condition monitoring and diagnostics scenario, simulation models of mechanical systems in faulty condition can be developed. System modeling is generally realized in order to estimate the influence of design and material modification on the vibration response (virtual prototyping) [14] but it can be also useful to evaluate the defect nature and its effect on the vibration response (diagnostics purposes) [15,16], as done in this paper. Different modeling approaches can be adopted, such as analytical model [17–20], finite element model [21,22] and multibody model [23,24]. Each model has to be validated fitting the numerical results with data collected experimentally.

In this paper, a quality control methodology to be used at the end of the production line for the identification of manufacture anomalies in heavy duty wheels is developed. The overall fault detection process (measurement and analysis) should not exceed 23 s in order to not delay the manufacturing process. Firstly, experimental tests have been carried out in order to select the best sensor typology (Section 3). Secondly, a single degree of freedom (SDOF) lumped parameter model of the heavy duty wheel is presented (Section 4). The model enables the physical explanation of the phenomena that cause the faulty signal signature as a function of operational conditions and defect size: this is important in order to select the suitable signal processing techniques to be used in the diagnosis step. Then in Section 5, different processing techniques have been applied to the heavy-duty wheel experimental signal: (i) synchronous average is calculated over the wheel rotation in order to highlight the phenomena that have wheel rotation as periodicity; (ii) Kurtosis and Root Mean Square parameters are utilized as statistical coefficients in order to define the state of health of a wheel and to obtain upper thresholds for the pass/fail decision; (iii) cyclostationary theory is applied to extract information from the frequency/order domain of the processed signal. Eventually, concluding remarks are given highlighting the suitable diagnostics tools.

The originality of this activity consists of the attempt to study the presence of anomalies in heavy-duty wheels and to compare the detection capability of synchronous average and cyclostationarity using well-suited indicators, through the support of a SDOF model.

2. Test set up

The wheels being studied are composed of a polyurethane tread and a cast iron hub, with 100 mm radius, 50 mm of width and 1200 kg of maximum load. The adhesive application between tread and hub is the most critical assembly phase,

Please cite this article as: M. Malago', et al., Fault detection in heavy duty wheels by advanced vibration processing techniques and lumped parameter modeling, Mech. Syst. Signal Process. (2015), http://dx.doi.org/10.1016/j.ymssp.2015.09.043

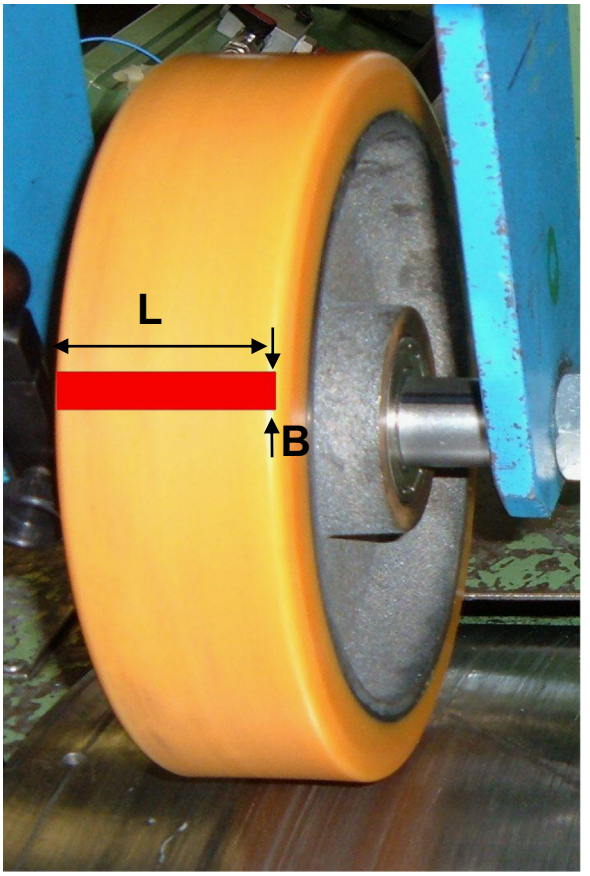

Fig. 1. Defect dimensions.

since it is completely done by an operator and a contamination of the bond area may happen. The operator has to be particularly careful to not touch the surface of the adhesive in order to prevent contamination with impurities that would lead to a fast failure of the polyurethane–hub adherence. If this processing phase is not properly executed some defects can arise as non-uniform adhesion of the adhesive on the metal surface or not complete wettability of the metal surface.

In this context, wheels with different types of faults have been manufactured ad hoc with anomalies similar to those that can really appear during the manufacturing process. Defects of missing glue between tread and hub have been realized (0.3 cm in the circumferential and axial direction, respectively "B" and "L" in Fig. 1). Subsequently, defects of different nature (rust presence in the hub surface) have been manufactured. These defects are described and examined hereafter:

1. Missing Adherence defect (namely MA): incorrect adherence zones between tread and hub of about 0.3 cm dimensions in the axial and circumferential directions; two wheels have been manufactured with this defect.
2. Localized Rust defect (namely LR): localized rust presence in the hub surface of about 5 cm dimension in axial and 2 cm in circumferential direction; three wheels have been manufactured with this defect.
3. Distributed Rust defect (namely DR): distributed rust on the entire hub; three wheels have been manufactured with this defect.

Moreover, a set of 15 wheels without any defect has been analyzed for the estimation of a reliable reference pattern. The vibration parameters relative to these 15 wheels are referred to as Healthy Wheels (HW).

A wide experimental investigation is carried out on heavy-duty wheels in a test bench available at the company's laboratory. The test bench consists of a bottom support, including a drum driven by an electric motor controlled by an inverter and an upper part composed of a horizontal cross beam and two hydraulic pistons that apply the load to the wheel under test, as depicted in Fig. 2. Tests are carried out at two different drum speeds (4 and 10 km/h) and three different loads (350, 700 and 1000 kg), representing the real range of operational conditions. During tests, the vibration signal is acquired by means of a piezoelectric tri-axial accelerometer (PCB 356A01, frequency range 1–10,000 Hz), as shown in Fig. 2 (position A) and a condenser microphone (1/2 in. prepolarized) is utilized to measure the sound emission (C). Moreover, an acoustic emission (AE) sensor has been used in order to capture the transient elastic waves generated from a rapid release of strain energy caused by a deformation or damage (B). The acoustic emission sensor is specifically manufactured for measuring the

Please cite this article as: M. Malago', et al., Fault detection in heavy duty wheels by advanced vibration processing techniques and lumped parameter modeling, Mech. Syst. Signal Process. (2015), http://dx.doi.org/10.1016/j.ymssp.2015.09.043

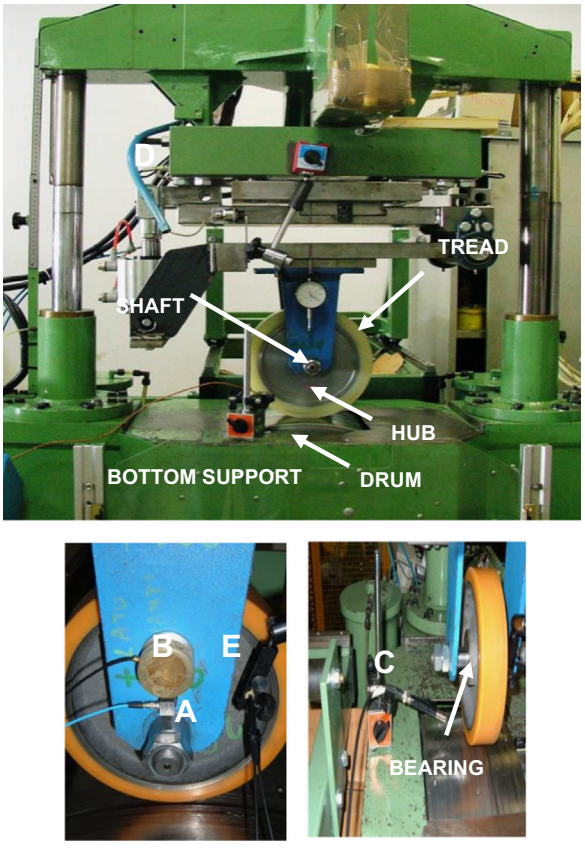

Fig. 2. Test bench: A) accelerometer ; B) acoustic emission sensor; C) microphone; D) load cells; E) optical tachometer sensor.

elastic waves which have high frequency content. Thus, such a sensor is negligibly affected by mechanical components that commonly have a low frequency content, less than 20 kHz [25,26]. Finally, four load cells (LAUMAS FTO Kg 5000) have been used to measure the global force in the vertical direction (D). The signals are acquired with a sample frequency of 12,800 Hz for a duration of about 23 s by using LMS hardware and software instrumentation (LMS Test.Lab and LMS Scadas III). The analysis time of 23 s was selected in order to not delay the manufacturing process, since the developed condition monitoring procedure should be placed at the end of the production line. Simultaneously with the acquisition at constant sample frequency, an on-line order tracking analysis has been also performed since the number of time samples varies every rotation of the wheel due to fluctuation of instantaneous speed. This technique requires the measurement of a trigger signal, i.e. a signal phase-locked with the angular position of one rotating element in the system that gives a synchronized signal with the wheel and a synchronized signal with the drum revolution. For these reasons, two optical tachometer sensors (KEYENCE- LVS series) both positioned near the wheel–drum contact are used in order to produce one pulse per revolution of the wheel and the driving drum (*E*). This kind of tachometer gives a pulse when a reflecting strip crosses the optical sensor of the tachometer.

After the experimental test described above, the entire set of wheels (faulty and healthy wheels) has been subjected to a peeling test in order to assess the presence of the defect for the faulty wheels and the absence of the defect in the healthy wheels.

3. Determination of the best sensor

Numerous experimental analyses have been carried out in order to detect which sensor among those used is able to identify at the best the non-stationary phenomena related to the defect presence.

Fig. 3 refers to the angular domain signals evaluated on the wheel rotation (defined in detailed in Section 5 as synchronous average of the wheel, SAw) at the operational condition of 4 km/h and 1000 kg and for the same defect type. This comparison leads to the conclusion that the accelerometer signal is the best compromise between simplicity in the mounting and clear response to an impulsive event. In fact, in the acceleration signal, the impulsive events which occur when the artificial fault of the wheel comes into contact with the drum are clearly depicted. On the other hand, the load cells embedded in the test bench are able to detect the presence of the defect, but its localization in circumferential direction

Please cite this article as: M. Malago', et al., Fault detection in heavy duty wheels by advanced vibration processing techniques and lumped parameter modeling, Mech. Syst. Signal Process. (2015), http://dx.doi.org/10.1016/j.ymssp.2015.09.043

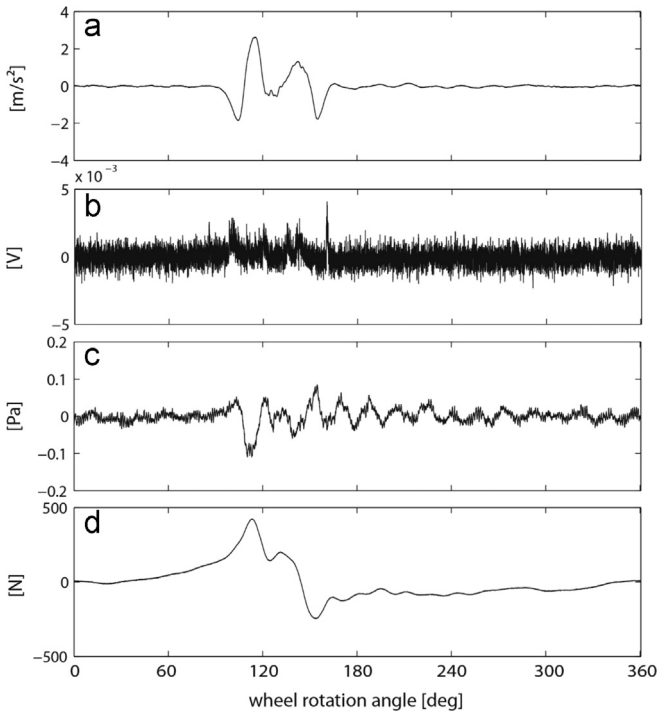

Fig. 3. Synchronous Average of a) accelerometer signal, b) AE signal, c) microphone signal, d) load cell signal for the same defect type of dimensions $B=2$ cm and L=5 cm at the operational condition of 4 km/h and 1000 kg.

is not as precise as the acceleration plot. AE exhibits quite good signals allowing defect localization; however, the main drawbacks linked to the use of this transducer are the requirement of a continuous control of the silicon grease, essential to realize good adherence between sensor and measured surface, and the high sensitivity to electrical interferences. Finally, microphone signals are not suitable for this kind of measurement due to the high environmental noise in the production line, although the signal depicted in Fig. 3 is rather good (measurement in a low noise laboratory). In the following, only the results obtained by the accelerometer will be analyzed and discussed.

4. Lumped parameter modeling

The developed single degree of freedom model comprises the heavy-duty wheel, support and horizontal cross beam and it is depicted in Fig. 4. The aim of the model is to qualitatively reproduce the acceleration signal considering the moving parts of the system (i.e. tread, hub, support and horizontal cross beam) as a unique rigid body and considering the contact patch as the flexible part. Thus, it will be possible to give a physical explanation of the two complete sine waves depicted in the experimental acceleration signal of Fig. 3a. This information can help in the selection of the suitable signal processing techniques for a fast and effective condition monitoring and diagnosis phase. Eq. (1) reports the selected governing equation of motion in case of visco-elastic material:

$$M\ddot{x}(t)+c\dot{x}(t)+k(t)x(t)^{e}=F \tag{1}$$

where x is the translational DOF in vertical direction, M is the moving mass comprising the mass of tread, hub, support and horizontal cross beam, c is the contact damping, F is the applied load, and $k(t)$ denotes the time-varying contact stiffness in case of defect presence while, in case of healthy wheel, the stiffness has to be considered constant in time. The constant contact stiffness in case of healthy wheel has been extracted from static deformation measurements conducted on the heavy duty wheel; during such a test, an oil film has been applied on the sample surfaces in order to reduce the clamping adhesion effect. Fig. 5 reports the load–strain hysteresis curve of the heavy duty wheel subjected to static load. Frequency and temperature dependencies have not been considered due to the low frequency content of the acceleration signal in case of defect presence and to the negligible temperature increase. The area within the hysteresis loop of Fig. 5, namely D, represents the dissipated energy per cycle of harmonic motion. For reasonable levels of damping, the loop area can be used to calculate damping factor ξ:

$$\xi=\frac{1}{2}\left(\frac{D}{\pi F_{max} d_{max}}\right) \tag{2}$$

Please cite this article as: M. Malago', et al., Fault detection in heavy duty wheels by advanced vibration processing techniques and lumped parameter modeling, Mech. Syst. Signal Process. (2015), http://dx.doi.org/10.1016/j.ymssp.2015.09.043

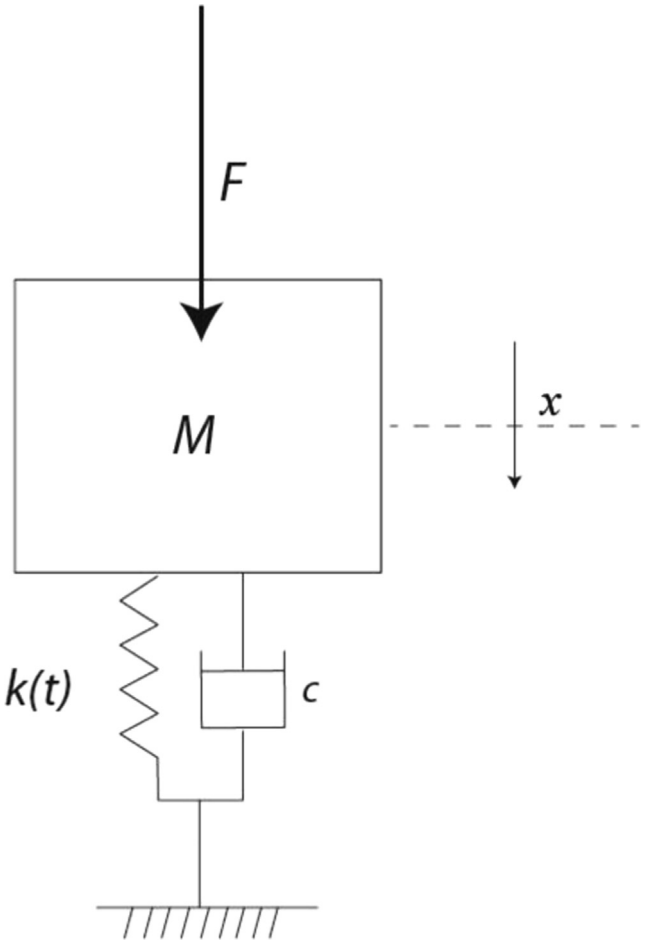

Fig. 4. One degree of freedom lumped parameter model.

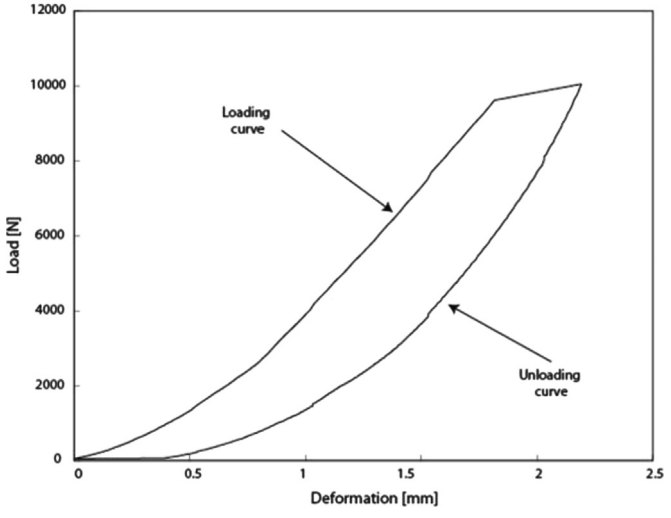

Fig. 5. Loading–unloading curve obtained through a static test conducted on a wheel.

where F_{max} and d_{max} are the maximum values of load and deformation of Fig. 5, giving a ξ value of around 0.1. Thus, damping

Please cite this article as: M. Malago', et al., Fault detection in heavy duty wheels by advanced vibration processing techniques and lumped parameter modeling, Mech. Syst. Signal Process. (2015), http://dx.doi.org/10.1016/j.ymssp.2015.09.043

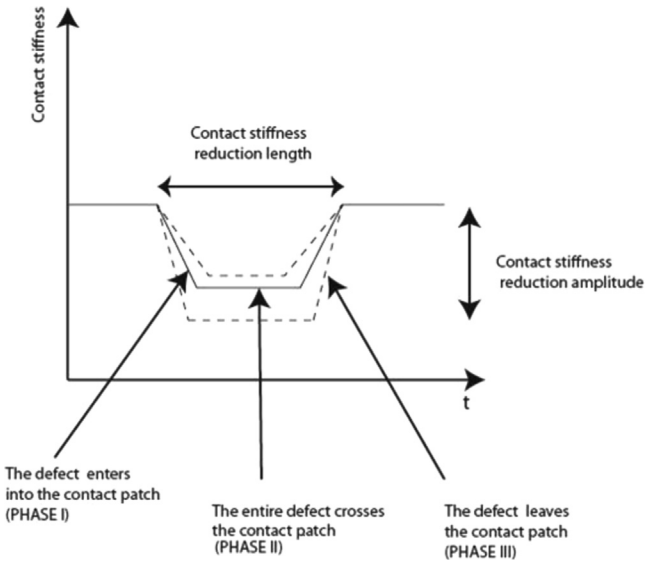

Fig. 6. Representation of the time-varying contact stiffness in case of missing adherence defect.

coefficient c of Eq. (1) has been evaluated through the assumption of proportional damping:

$$c = 2\xi\sqrt{kM} \tag{3}$$

Exponent e of Eq. (1) has been evaluated fitting the loading curve of the hysteresis cycle. This parameter represents the non-linear behavior of polyurethane composing the tread material. Finally, force F is the constant force applied by the hydraulic system to the global moving mass. Global mass M is 38 kg, the constant values of the contact stiffness k is $4 \cdot 10^6$ N/m^e and non-linear exponent e is equal to 1.58.

In order to simulate the acceleration signal in case of faulty condition, the time-varying contact stiffness should be defined a priori. In case of defect, the contact stiffness is expected to vary over time as depicted in Fig. 6; in particular, it is expected that the contact stiffness is reduced with respect to the healthy condition. When the defect zone enters into the contact patch the contact stiffness decreases (PHASE I). Then, as long as the defect zone is within the contact patch (PHASE II), the contact stiffness has the minimum value. Eventually, the contact stiffness increases when the defect starts to leave the contact patch (PHASE III). The time extension of the three phases can vary, depending on the defect types and on the operational conditions. Such a qualitative and simplified representation of the fault in terms of contact stiffness can be useful in order to explain the nature of the measured signal, as shown in Section 4.1. The contact stiffness reduction has been estimated in agreement with the experimental acceleration results. Although the three phases occur every wheel rotation, i.e. when the defect area comes into contact with the contact patch, the fault presence cannot be assumed as a purely periodic event.

In case of a localized missing adherence defect, the measured signal is expected to be composed of a deterministic and a non-deterministic part. The deterministic part is related to the phenomena periodic with the wheel rotation; in this case, the contact stiffness varies when the defect enters and exits from the contact patch. A non-deterministic part due to the inevitable presence of slip phenomena originates in the contact between the polyurethane tread and drum.

In case of rust defects, the presence of rust reduces the adherence between tread and hub. However, the quantity of rust along the circumferential and axial direction is not controlled during the defect manufacturing process. For this reason the contact stiffness variation law is hardly predictable; moreover, the entry and exit of the defect from the contact patch can be expected to be characterized by a high randomness and it cannot be thought of a stable phenomenon. On the contrary, the missing adherence defect is manufactured by excluding a portion of hub surface from the glue; this procedure determines a perfect non adherence between hub and tread and thus a well-defined stiffness variation law. In case of rust defects, the measured signal can be considered as composed of a deterministic part, due to the periodic entry and exit of the defect from the contact patch and a significant non-deterministic part; indeed, when the rust area enters into the contact patch, the contact stiffness exhibits random variations, leading to random system excitations.

4.1. *Influence of operational condition and defect size*

Heavy-duty wheels under operational conditions are normally characterized by variable loads and speeds: loads can vary between 350 and 1000 kg with speed between 4 and 10 km/h. In the following, different operational conditions and defect sizes have been experimentally and numerically analyzed in order to understand the meaning of the signal signature. Note that the experimental synchronous averages reported in this subsection have been obtained with 80 averages over the

Please cite this article as: M. Malago', et al., Fault detection in heavy duty wheels by advanced vibration processing techniques and lumped parameter modeling, Mech. Syst. Signal Process. (2015), http://dx.doi.org/10.1016/j.ymssp.2015.09.043

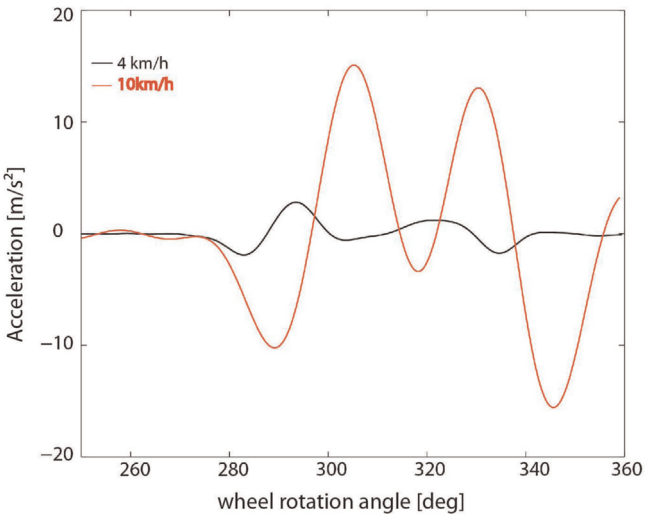

Fig. 7. Synchronous average of the experimental accelerations measured at the operational load of 1000 kg, missing adherence defect size of $L=5$ cm, $B=2$ cm and at speeds of 4 km/h and 10 km/h.

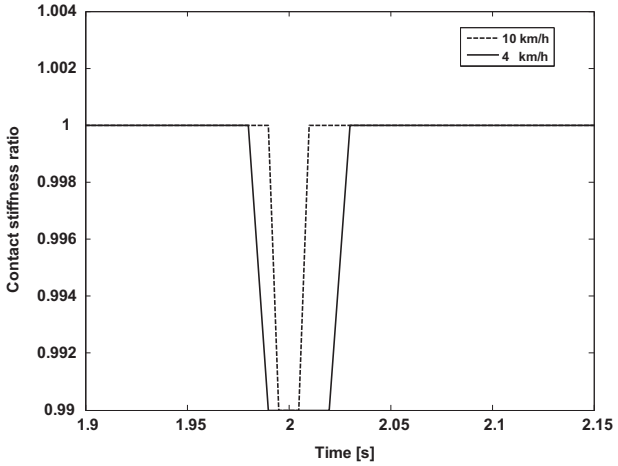

Fig. 8. Sketch of the contact stiffness ratio between the faulty and healthy case, in the time domain at 4 km/h and 10 km/h in case of the same missing adherence defect dimension of $B=5$ cm and $L=2$ cm.

wheel rotation (referred as *Saw* and defined in Section 5) in order to reduce the noise-to-signal ratio leading to a clearer understanding of the dynamic phenomena.

The vibration signal is highly influenced by rotational speed. Fig. 7 reports the experimental *SAw* in case of defect size of $B=2$ cm and $L=5$ cm at two different speeds (4 and 10 km/h) and 1000 kg of load. The system appears to be significantly more excited at higher velocity: the acceleration signal amplitude is increased as well as the angular range. In order to represent the speed effect on the SDOF model, it is necessary to hypothesize a particular law of the contact stiffness variation. Fig. 8 shows the contact stiffness ratio between the faulty and healthy case in the time domain at the operational speeds of 4 and 10 km/h: the stiffness variation is expected to become more impulsive as the speed increases in agreement with the experimental results reported in Fig. 7. The value of 0.99 of contact stiffness ratio has been estimated by comparison between the amplitude of the measured and simulated acceleration signals. In particular, if the wheel rotates at higher speed, the time needed by the defect to enter, to pass and to exit from the contact patch is expected to be reduced, giving a sharper stiffness variation, and consequently, a more impulsive system excitation. This is also highlighted by the results of the lumped parameter model reported in Fig. 9(a): in the defect zone, at about 170°, the two simulated accelerations are considerably different in terms of amplitude and angular extension. It is interesting to note that Fig. 9(b) reports the relative stiffness variation due to the defect in terms of wheel rotational angle. In this case, the stiffness variation remains the same for the two rotational speeds (4 and 10 km/h) since it is represented in the angular domain of the wheel rotation; on the contrary, in Fig. 8 the stiffness variation was represented as a function of time and the stiffness variations were different for the 4 and 10 km/h scenario. Again, the value of 0.98 of contact stiffness ratio has been estimated by

Please cite this article as: M. Malago', et al., Fault detection in heavy duty wheels by advanced vibration processing techniques and lumped parameter modeling, Mech. Syst. Signal Process. (2015), http://dx.doi.org/10.1016/j.ymssp.2015.09.043

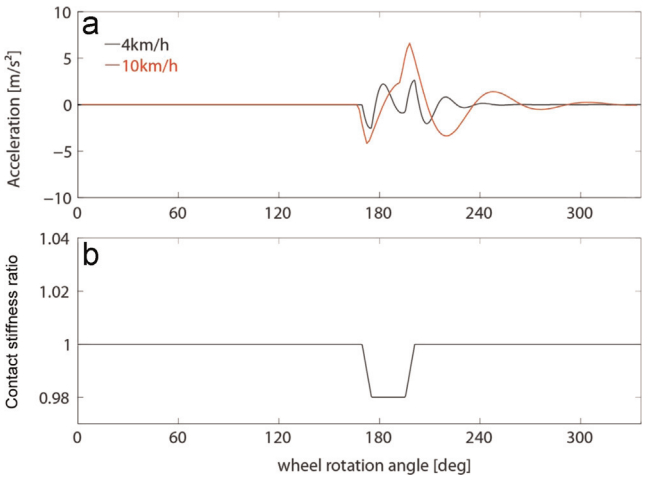

Fig. 9. Numerical acceleration (a) and contact stiffness ratio between the faulty and healthy case (b) at the operational load of 1000 kg, missing adherence defect size of $L=5$ cm, $B=2$ cm and at speeds of 4 km/h and 10 km/h.

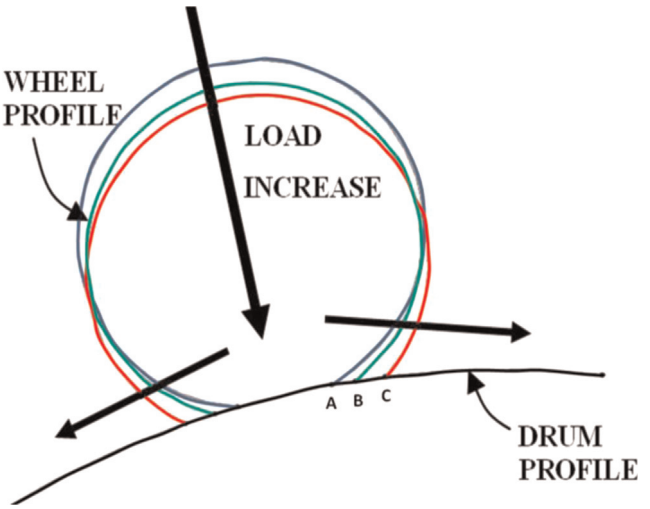

Fig. 10. Sketch of the contact patch changing extension at different applied loads.

comparison between the amplitude of the measured and simulated acceleration signals; in particular, the value of 0.99 refer to $L=5$ cm defect dimension while 0.98 refers to $L=2$ cm defect dimension.

Load conditions produce a different influence on signal behavior. Fig. 10 sketches the variation of the contact area between wheel and drum at different load conditions. Points A, B and C highlight the variation of the contact point at different loads. In particular, point A represents the low load condition for which less contact surface and wheel angle are involved in the contact. On the other hand, point C represents the high load condition that determines larger contact area and larger wheel angle involved. Fig. 11 shows the experimental vibration signal obtained for missing adherence defects of 2 cm extension in circumferential direction and 5 cm in axial direction at three different loads (350, 700 and 1000 kg). It is clear that the acceleration waveform has a higher amplitude when the load increases. Moreover, taking Fig. 11 as a reference, at 1000 kg, the first negative peak at about 280° occurs before the corresponding peaks for the other lower loads; on the other hand, at 1000 kg, the last negative peak at about 335° occurs after the corresponding peaks for the other lower loads. Thus, the angular extension of the waveform is slightly larger as supposed in Fig. 10. Once again, it is necessary to hypothesize a stiffness variation law in order to reproduce the load effect on the model. The contact patch at different load conditions has been experimentally measured: the wheel external surface has been painted and the different loads have been applied. The imprint left by the wheel is the effective dimension of the contact patch. Such values have been included in the model in terms of angular domain and the load influence on the acceleration signal has been qualitatively modeled by an angular extension variation of the stiffness (see Fig. 12(b)). Fig. 12(a) reports the numerical results obtained considering different stiffness variations, in case of a same defect extension. In the defect zone, at about 270°, the load condition slightly affects the acceleration amplitude and the angular range, in agreement with the experimental results (Fig. 11). In particular,

Please cite this article as: M. Malago', et al., Fault detection in heavy duty wheels by advanced vibration processing techniques and lumped parameter modeling, Mech. Syst. Signal Process. (2015), http://dx.doi.org/10.1016/j.ymssp.2015.09.043

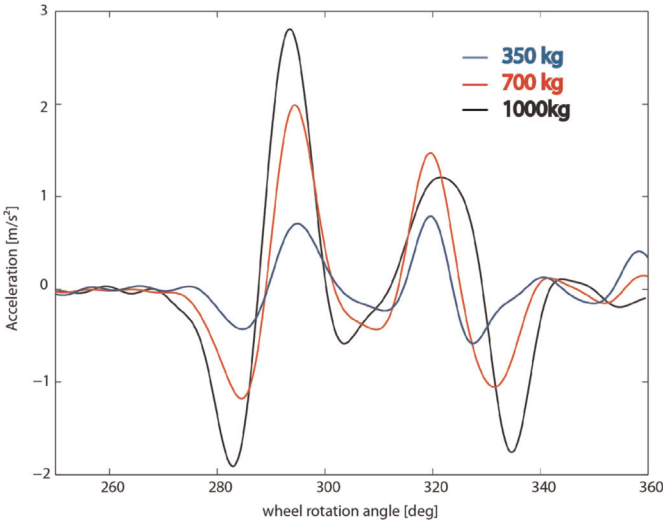

Fig. 11. Synchronous average of the experimental acceleration measured at the operational speed of 4 km/h, missing adherence defect size of $L=5$ cm, $B=2$ cm and at load conditions of 350 kg, 700 kg and 1000 kg.

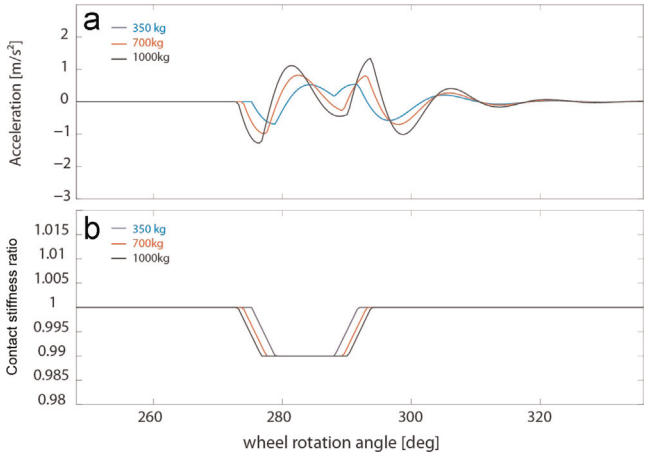

Fig. 12. Numerical acceleration (a) and contact stiffness ratio between the faulty and healthy case (b) at the operational speed of 4 km/h, missing adherence defect size of $L=2$ cm, $B=2$ cm and load conditions of 350 kg, 700 kg and 1000 kg.

due to the different angular extension of the stiffness variation as a function of the load, the resulting acceleration signal is still dependent on the load, as occurs for the experimental acceleration (see Figs. 11 and Fig. 12(a)).

The effect of the missing adherence defect size is also considered. In particular it has been experimentally found that the effect of the axial extension (L) in terms of acceleration amplitude is considerably more important compared with the circumferential extension (B), as reported in Fig. 13. The different axial extension of the defect has been qualitatively represented into the model by a stiffness reduction with respect to the healthy condition. In order to estimate the suitable stiffness percentage reduction, the numerical acceleration signal has been fitted with the experimental data considering, for a width extension of 5 cm, a contact stiffness ratio reduction of around 2% from the healthy value k. In case of smaller defect extension, e.g. 2 cm, the percentage stiffness variation has been reduced to 1% , causing a smaller acceleration amplitude, Fig. 14.

5. Application of advanced signal processing techniques

In this section, advanced signal processing techniques have been used in order to identify the presence of defects. The advanced signal processing techniques have been applied to the raw time data of the 15 healthy wheels and 8 faulty wheels described in Section 2, at the operational condition of 4 km/h and 1000 kg. This operation condition has shown to be the

Please cite this article as: M. Malago', et al., Fault detection in heavy duty wheels by advanced vibration processing techniques and lumped parameter modeling, Mech. Syst. Signal Process. (2015), http://dx.doi.org/10.1016/j.ymssp.2015.09.043

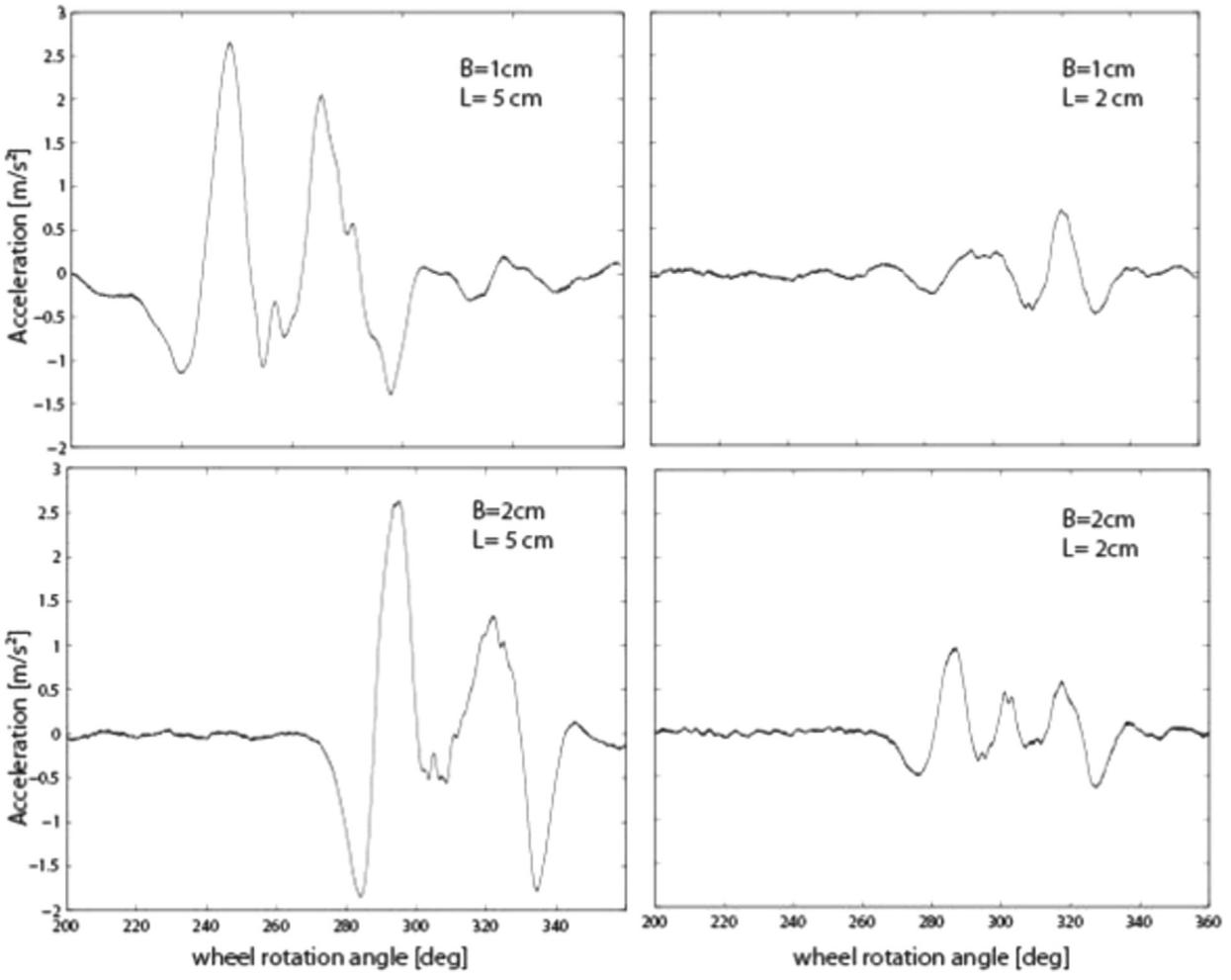

Fig. 13. Synchronous average of the experimental acceleration of 4 different wheels measured at the operational speed of 4 km/h, operational load of 1000 kg and with different missing adherence defect sizes in the axial and circumferential directions.

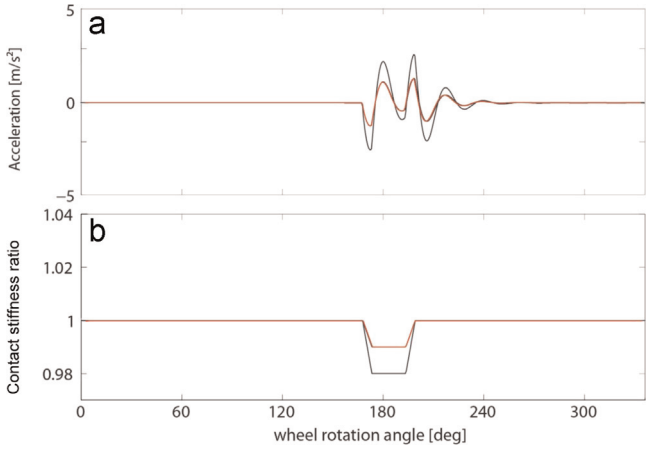

Fig. 14. Numerical acceleration (a) and contact stiffness ratio between the faulty and healthy case (b) at the operational speed of 4 km/h, operational load of 1000 kg and at different defect sizes in the axial direction.

Please cite this article as: M. Malago', et al., Fault detection in heavy duty wheels by advanced vibration processing techniques and lumped parameter modeling, Mech. Syst. Signal Process. (2015), http://dx.doi.org/10.1016/j.ymssp.2015.09.043

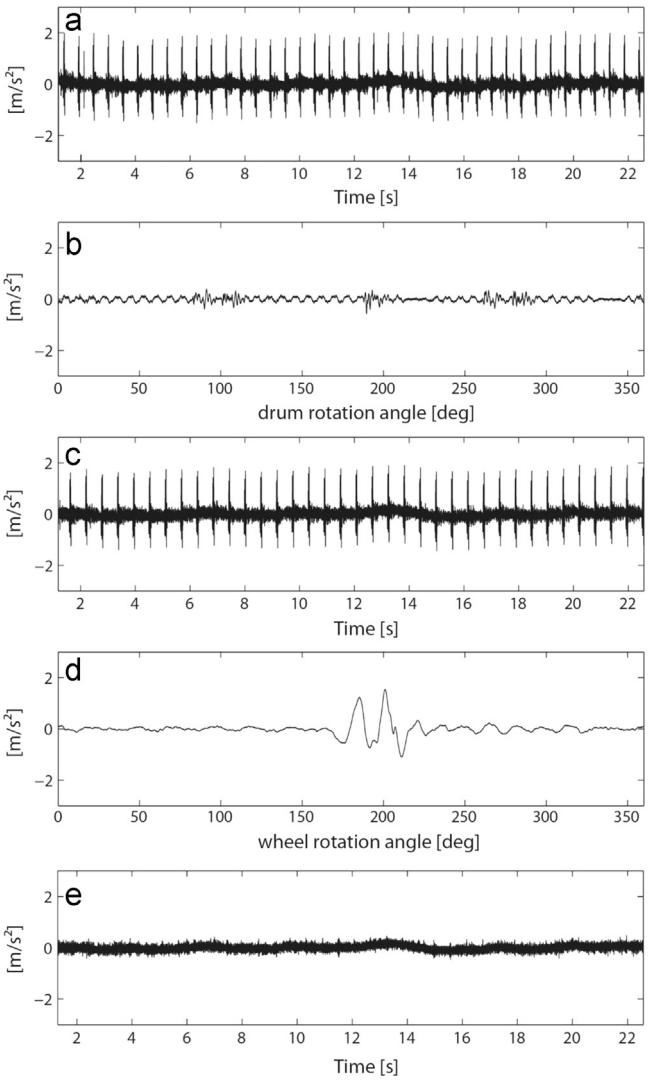

Fig. 15. Processing procedure: a) raw acceleration signal, b) SAd, c) purified signal, d) SAw and e) residual signal at the operational condition of 4 km/h and 1000 kg.

best compromise (referred hereafter as "best" condition) of rotational speed and applied load in order to give a clear and meaningful response signal.

5.1. Synchronous average analysis

The Synchronous Average (SA) technique has been applied on the measured signals in order to highlight the phenomena that are linked to the presence of faulty wheels. The Synchronous Average $m_x(\vartheta)$ of a measured signal $x(\vartheta)$, synchronized with the rotational element in the angle domain ϑ, is evaluated as the ensemble average over a number of rotations M, each corresponding to one angular period $\Theta = 360°$, as follows:

$$m_x(\vartheta) = \frac{1}{M}\sum_{l=0}^{M-1} x(\vartheta + l\Theta), \quad \text{with } 0 \le \vartheta < \Theta \tag{4}$$

where $M\Theta$ is the whole length of the signal. Synchronous Average (SA) is a well adopted signal processing technique which enables periodic waveforms to be extracted from noisy signals.

Hereafter, the different processing techniques used for the estimation of the SA used in this paper are detailed. Moreover, Fig. 15 depicts the results of the procedure

complete procedure developed for the time signal purification is detailed and Fig. 15 depicts the different processed signals.

Please cite this article as: M. Malago', et al., Fault detection in heavy duty wheels by advanced vibration processing techniques and lumped parameter modeling, Mech. Syst. Signal Process. (2015), http://dx.doi.org/10.1016/j.ymssp.2015.09.043

Two different SA have been computed: the Synchronous Average of the acceleration signal over the drum revolution (called *SAd*) and Synchronous Average of the acceleration signal over the wheel revolution (called *SAw*). The procedure in order to estimate such Synchronous Averages and to purify the raw time signal is hereafter detailed, taking Fig. 15 as a reference. In particular, Fig. 15 depicts the raw acceleration signal measured at the operational condition of 4 km/h and 1000 kg in the case of a missing adherence localized defect and the further processing phases.

Firstly, the Synchronous Average of the acceleration signal over the drum revolution (called *SAd*) is calculated (Fig. 15(b)); it has been performed starting from the synchronized acceleration signal, i.e. from the raw acceleration signal after resampling in the angle domain by using the tachometer signal of the drum as a reference. It is presented in the angle domain, since it is a Synchronous Average. Note that the angle domain regards one revolution of the drum, which corresponds to about 3 revolutions of the wheel.

Secondly, the "purified signal" depicted in Fig. 15(c) is calculated as the difference between the synchronized acceleration signal (i.e. the raw acceleration signal after resampling in the angle domain by using the tachometer signal of the drum as a reference) and the *SAd*, obtaining a new signal with reduced periodicities related to the driving drum and increased information concerning the manufactured faults linked to the wheel periodicities. This new signal is then presented in the time domain after resampling from angle to time (by using the tachometer signal of the drum as a reference). The "purified signal" is presented in the time domain with the aim to be simply compared with the raw acceleration signal.

Thirdly, the Synchronous Average of the acceleration signal over the wheel revolution (namely *SAw*) is estimated (Fig. 15(d)). The "purified signal" has been synchronized by using the tachometer signal of the wheel and averaged over the wheel rotation obtaining the *SAw*. It is presented in the angle domain and in particular for one revolution of the wheel. Here, the *SAw* is obtained starting from the "purified signal" instead of the raw signal as usually; thus, the presence of noise in such a *SAw* is reduced even after few averages.

Finally, the residual signal depicted in Fig. 15(e) was determined as the difference between the "purified signal" synchronized by using the tachometer of the wheel and the *SAw*. The residual signal is then presented in the time domain after resampling from angle to time (by using the tachometer signal of the wheel). The residual signal is presented in the time domain for a fast comparison with the raw and the "purified signal".

Such a "purification process" gives a strong reduction of the components related to the driving drum rotation and the possibility of analyzing the residual signal cleaned of all the known periodicities.

The Kurtosis parameter can be considered as a monitoring feature for faults producing impulsive excitations and it can be used to obtain a reliable upper threshold [27]. The use of the Kurtosis statistical parameter on the *SAw* was also suggested by the results of the LP model (Section 4). Due to the shape and meaning of the simulated signals (Figs. 12 and 14) as a function of operational parameters, the Kurtosis parameter could enable diagnostic insights for localized defects at least. Although this parameter is well suited for the recognition of extended missing adherence localized faults, it is not really sensitive to small localized defects (MA) and to rust presence (LR and DR), as it shows almost the same value as healthy wheels, (see Figs. 16 and 17). Consequently, a further statistical parameter, the root mean square (RMS), has been considered and compared to the previous one. The RMS is a statistical metric able to recognize the degree of irregularity of a signal and for this reason it appears well-suited for the recognition of defects such as rust or small localized defects that do not produce

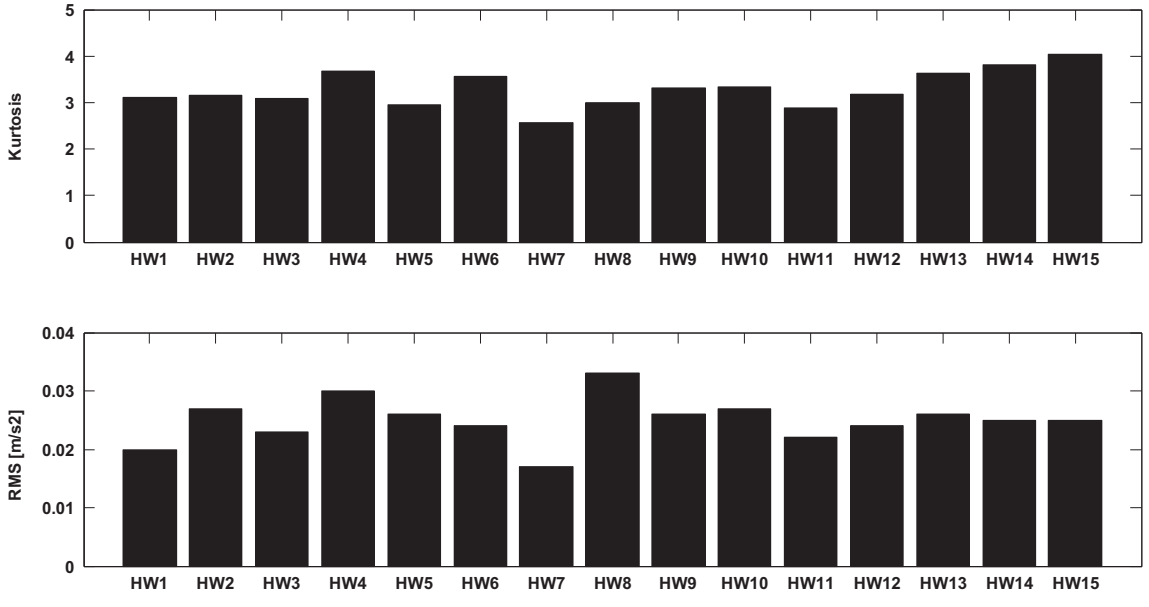

Fig. 16. Kurtosis and RMS values for the group of 15 healthy wheels at the "best" test conditions.

Please cite this article as: M. Malago', et al., Fault detection in heavy duty wheels by advanced vibration processing techniques and lumped parameter modeling, Mech. Syst. Signal Process. (2015), http://dx.doi.org/10.1016/j.ymssp.2015.09.043

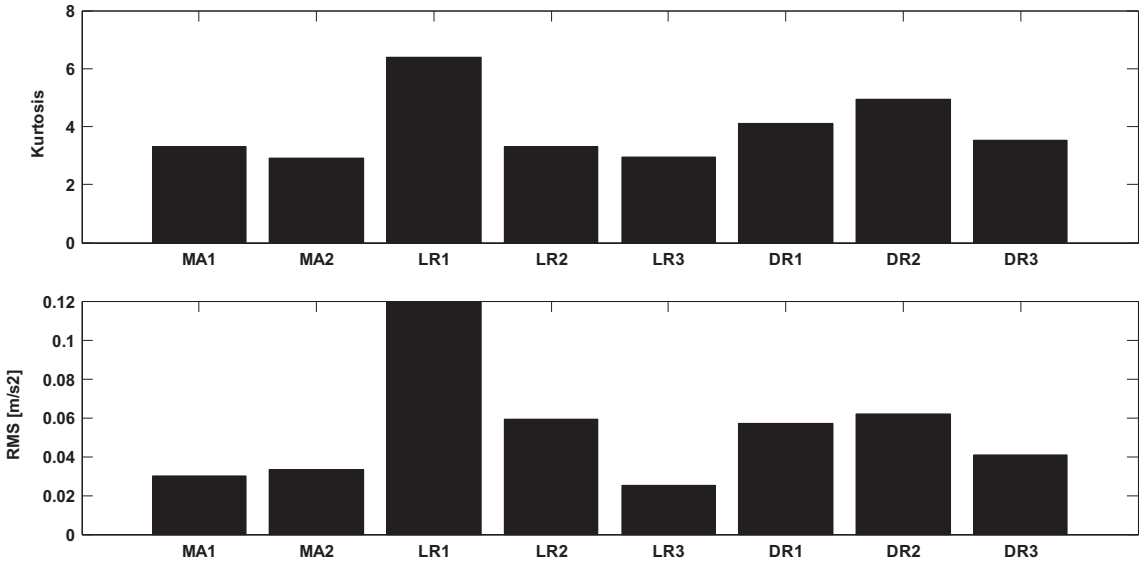

Fig. 17. Kurtosis and RMS values for the group of 8 different faulty wheels at the "best" test conditions.

Table 1
Kurtosis and RMS threshold values obtained using the Tukey's method at the "best" test conditions.

Healthy wheels (HW)	*Kurtosis*	*RMS [m/s^2]*
Q1	**3**	**0.023**
Q2	**3.17**	**0.025**
Q3	**3.62**	**0.027**
$Q_3+1.5\lvert Q_3-Q_1\rvert$	**4.55**	**0.033**
$Q_3+3\lvert Q_3-Q_1\rvert$	**5.48**	**0.039**

significant localized peaks. The RMS values computed on the *SAw* for the group of 15 healthy wheels and for the group of 8 faulty wheels are collected in Figs. 16 and 17, respectively.

Finally, Tukey's method has been applied to the Kurtosis and RMS parameters evaluated for the group of healthy wheels (Fig. 16) in order to identify the pass/fail threshold value. Let $x_1, x_2, \ldots, x_n$ be a series of observations such as statistical parameter values or cyclostatonarity indicators. These data are arranged in ascending order and then ordered into four quarters. The boundary of each quarter is defined by Q_1, Q_2 and Q_3, called the 1st quartile, 2nd quartile and 3rd quartile, respectively. The difference $|Q_3-Q_1|$ is called the inter-quartile range. The Tukey's threshold for anomalies is defined as $Q_3+3|Q_3-Q_1|$. Observations falling beyond this limit are called serious anomalies and any observations x_i (i=1,2,…n) such that $Q_3+1.5|Q_3-Q_1| \le x_i \le Q_3+3|Q_3-Q_1|$ are called possible anomalies. With this approach, the threshold value that discriminates healthy wheel from a possible faulty wheel has Kurtosis of 4.55 and RMS of 0.033 m/s^2 (accordingly to the method). The thresholds that give the certainty of faultiness are 5.48 and 0.039 m/s^2 for the Kurtosis and the RMS, respectively, as reported in Table 1. The comparison of the pass/fail threshold value (Table 1) with the results reported in Fig. 17 enables to draw the following conclusions, as highlighted in Fig. 18:

1. The Kurtosis parameter is able to certainly identify only one wheel with LR fault (LR1) and one wheel with DR fault (DR2) as a possible fault. This low monitoring skill can be ascribed to the fact that the *SAw* signals do not contain high localized peaks, in case of MA, LR and DR defects.
2. The RMS parameter is able to certainly identify two wheels with LR fault (LR1, LR2) and the three wheels with DR fault (DR2, DR3, DR4). Moreover, one wheel with MA fault (MA2) was recognized as possibly faulty. As a result the RMS can be considered as a good monitoring parameter since it is sensitive to missing adherence localized defect or localized-distributed rust. Nevertheless, this parameter is not able to recognize all the defects giving the possibility of undesirable alarms.

These results were expected, based on the conclusions of the LP model: the significant non-deterministic part of the acceleration signal for LR and DR defects cannot be estimated by statistical metrics like Kurtosis. In order to give a complete overview of the effectiveness of the statistical metrics, other statistical parameters have been investigated (e.g. maximum signal amplitude, standard deviation, crest factor, etc). Results are not reported in this paper. However, it can be concluded

Please cite this article as: M. Malago', et al., Fault detection in heavy duty wheels by advanced vibration processing techniques and lumped parameter modeling, Mech. Syst. Signal Process. (2015), http://dx.doi.org/10.1016/j.ymssp.2015.09.043

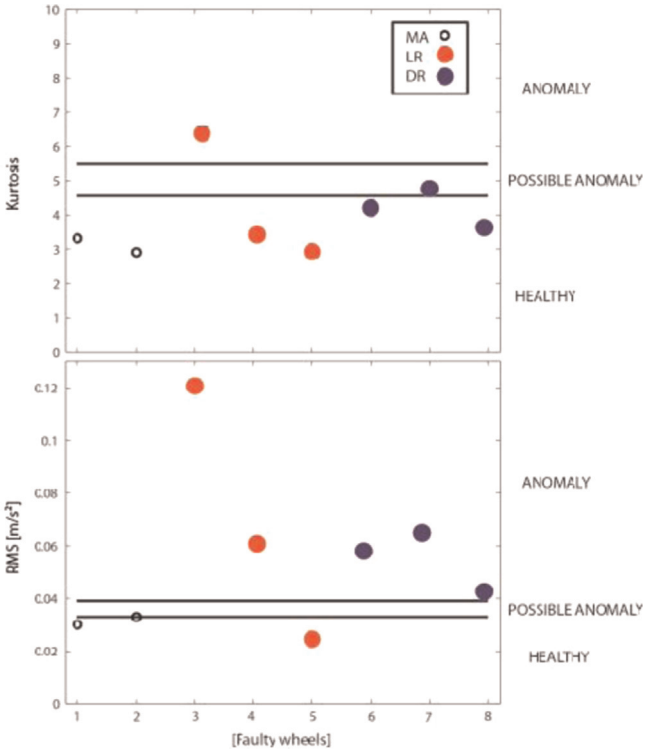

Fig. 18. Kurtosis and RMS pass–fail distributions in case of MA, LR and DR defects.

that statistical metrics are not effective for certain identification of the defects being tested; their monitoring skill is limited to a few defects. These metrics are not able to recognize all the defects.

5.2. Cyclostationary analysis

A further investigation has been carried out based on the study of cyclostationarity properties of the signal. The first order cyclostationarity content has been computed as the Discrete Fourier Transform (DFT) of the sampled purified signal synchronized with the wheel rotation $x[n]$, called first order cyclic cumulant ($\hat{C}_{1x}^{\alpha}$) [28–30]:

$$\hat{C}_{1x}^{\alpha} = N^{-1} DFT\{x[n]\}(\alpha) \tag{5}$$

The second order cyclostationarity content of the signal has been evaluated through the second order cyclic cumulant ($\hat{C}_{2x}^{\alpha}$) estimated as the Discrete Fourier Transform of the squared residual signal $r^2[n]$:

$$\hat{C}_{2x}^{\alpha}(0) = N^{-1} DFT\{r^2[n]\}(\alpha) \tag{6}$$

It has to be noted that Eqs. (5) and (6) are consistent estimators of the cyclic cumulants at the zero angle lag ($\varphi = 0$) for a sampled signal. Moreover, the first and second order cyclic cumulants can be conveniently used to summarize the information related to first- and second-order cyclostationary contents by defining the following indicators of cyclostationarity [3]:

$$ICS_{1x} = \frac{\sum_{\alpha \neq 0} \left|\hat{C}_{1x}^{\alpha}\right|^2}{\left|\hat{C}_{2x}^{0}(0)\right|} \tag{7}$$

$$ICS_{2x} = \frac{\sum_{\alpha \neq 0} \left|\hat{C}_{2x}^{\alpha}(0)\right|^2}{\left|\hat{C}_{2x}^{0}(0)\right|^2} \tag{8}$$

where $\alpha \in \overline{A}$ and $\overline{A}$ is the set of wheel orders α presenting non-zero Fourier series coefficients. It is worth noting that indicators ICS_{1x} and ICS_{2x} are dimensionless, as they are normalized by the energy of residual signal $\hat{C}_{2x}^{0}(0)$; they quantify the

Please cite this article as: M. Malago', et al., Fault detection in heavy duty wheels by advanced vibration processing techniques and lumped parameter modeling, Mech. Syst. Signal Process. (2015), http://dx.doi.org/10.1016/j.ymssp.2015.09.043

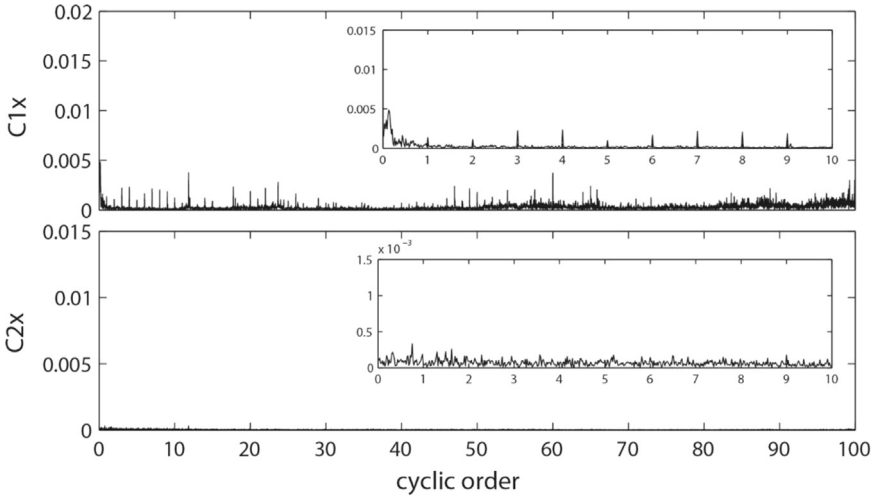

Fig. 19. $\hat{C}_{1x}^{\alpha}$ and $\hat{C}_{2x}^{\alpha}$ of depurated acceleration signal in case of healthy wheel at 4 km/h and 1000 kg.

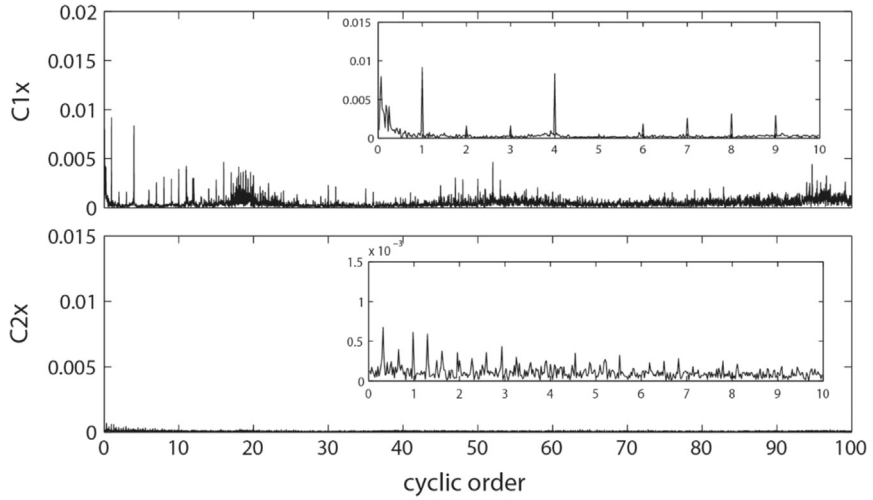

Fig. 20. $\hat{C}_{1x}^{\alpha}$ and $\hat{C}_{2x}^{\alpha}$ of depurated acceleration signal in case of MA faulty wheel at 4 km/h and 1000 kg.

presence of first and second-order cyclostationary components within the signal, respectively. In the particular case, α has been considered in the range 1st–100th order since the higher spectrum amplitudes lie in this order range.

Fig. 19 reports the first and second order cyclic cumulants in case of a healthy wheel while Fig. 20 does for a MA faulty wheel. Moreover, Fig. 21 reports the first and second order cyclic cumulants for a LR faulty wheel and Fig. 22 for a DR faulty wheel. For each figure, a zoom in the first 10 orders is also given representing the most significant signal contents range. Moreover, Figs. 23 and 24 report the cyclostationarity indicator values in the case of healthy and faulty wheels, respectively. Note that the cyclic cumulants depicted in Fig. 20, Fig. 21, Fig. 22 refer to a particular wheel, but they are representative of the whole set of healthy or faulty wheels.

Regarding the first cyclic order cumulant, it is interesting to note the presence of a high first order component and subsequent harmonics in the case of a localized defect of missing adherence (MA) with respect to the healthy condition. In the case of localized and distributed rust defects (LR and DR) the main differences from the healthy case are registered in both the first and in the second order cyclic cumulant.

As done for the statistical parameters, the Tukey's method has been applied to theand metrics evaluated for the group of 15 healthy wheels (Table 2) in order to identify the threshold pass/fail values. Possible faults can occur for values between 0.0893 and 0.1226 in the case of ICS_{1x} and for values between 0.0167 and 0.208 for ICS_{2x} metrics. Moreover assured faults can occur for values exceeding 0.1226 and 0.0208 for and , respectively. The comparison between the results in Fig. 24 and Table 2 leads to the following remarks, highlighted in Fig. 25.

Please cite this article as: M. Malago', et al., Fault detection in heavy duty wheels by advanced vibration processing techniques and lumped parameter modeling, Mech. Syst. Signal Process. (2015), http://dx.doi.org/10.1016/j.ymssp.2015.09.043

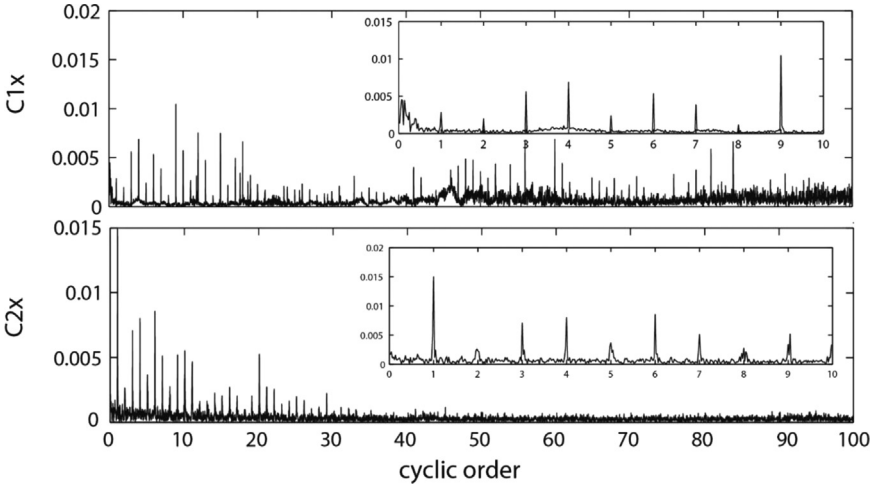

Fig. 21. $\hat{C}_{1x}^{\alpha}$ and $\hat{C}_{2x}^{\alpha}$ of depurated acceleration signal in case of LR faulty wheel at 4 km/h and 1000 kg.

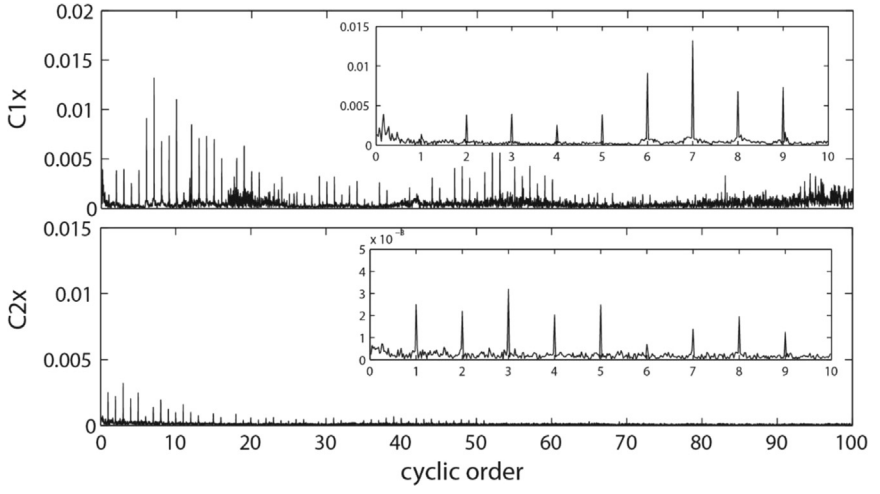

Fig. 22. $\hat{C}_{1x}^{\alpha}$ and $\hat{C}_{2x}^{\alpha}$ of depurated acceleration signal in case DR faulty wheel at 4 km/h and 1000 kg.

1. the ICS_{1x} parameter is able to detect only two certain faults (*LR*1 and *DR*2). Nevertheless this low monitoring skill is not really representative for the real differences between healthy and faulty wheels, as clearly appears when looking at the first order cumulants of Figs. 20–22. The main reason for this apparent discrepancy between the monitoring capability of the first cyclic order cumulant and its indicator is due to the large value of dispersion characterizing the healthy wheel, which causes a large increase of the threshold level.
2. the ICS_{2x} is able to recognize the presence of anomalies or of possible anomalies for all the known faulty wheels, in the case of both missing adherence and rust defect. In case of healthy components, the ICS_{2x} values do not present this dispersion effect so, as a result, the ICS_{2x} monitoring skill is particularly sensitive to fault recognition.

6. Concluding remarks

This research addresses a methodology and a procedure for the fault detection of heavy-duty wheels based on vibration measurements, passing through a simplified explanation of the physical phenomena that cause the faulty signal signature. Although this method and relative results are referred in this paper to wheels, they can be applied to a large variety of mechanical systems and give useful guidelines for similar applications.

A simplified approach aimed at the comprehension of the phenomena related to the missing adherence defect is proposed. A single degree of freedom model has been developed. The model is able to qualitatively simulate the vertical acceleration signal in case of localized missing adherence defect; moreover, the model allows the signal signature to be explained depending on the defect size and operational conditions. The model parameters have been experimentally obtained. The defect presence has been modeled as a stiffness reduction with respect to the healthy case. The model can be

Please cite this article as: M. Malago', et al., Fault detection in heavy duty wheels by advanced vibration processing techniques and lumped parameter modeling, Mech. Syst. Signal Process. (2015), http://dx.doi.org/10.1016/j.ymssp.2015.09.043

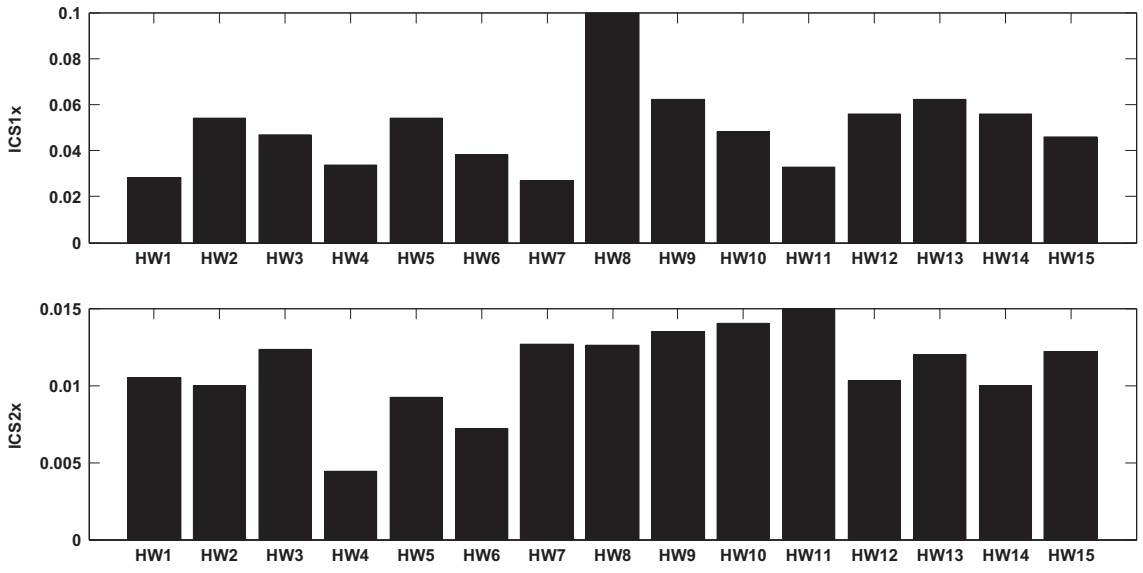

Fig. 23. ICS_{1x} and ICS_{2x} values for the 15 healthy wheels at the "best" test conditions.

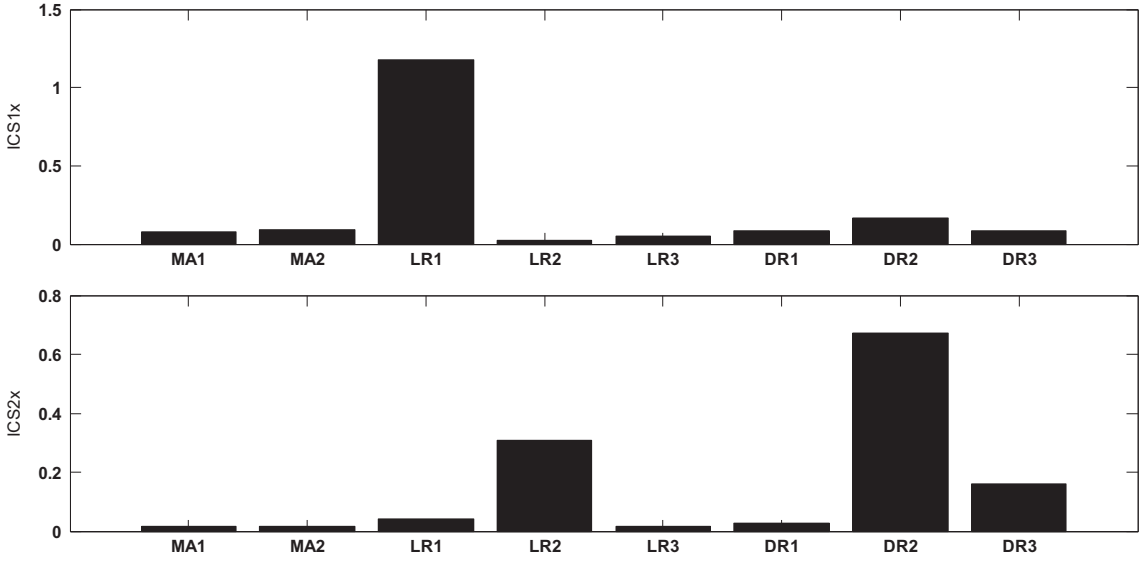

Fig. 24. ICS_{1x} and ICS_{2x} values for a group of 8 different faulty wheels at the "best" test conditions.

Table 2
ICS_{1x} and ICS_{2x} threshold values obtained using the Tukey method at the "best" test conditions.

Healthy wheels (HW)	ICS_{1x}	ICS_{2x}
Q1	**0.0338**	**0.01**
Q2	**0.0480**	**0.012**
Q3	**0.056**	**0.0127**
$Q_3+1.5\lvert Q_3-Q_1\rvert$	**0.0893**	**0.0167**
$Q_3+3\lvert Q_3-Q_1\rvert$	**0.1226**	**0.0208**

considered a useful tool for the interpretation of the experimental results and for the comprehension of the efficiency of the proposed processing techniques.

A number of different processing techniques are developed and applied in order to recognize faults in heavy-duty wheels. Defects of different dimensions reproducing missing adherence between the polyurethane tread and the hub are artificially created. These defects cause incorrect wheel rotations and fast failure. The synchronous average (SAw) has been

Please cite this article as: M. Malago', et al., Fault detection in heavy duty wheels by advanced vibration processing techniques and lumped parameter modeling, Mech. Syst. Signal Process. (2015), http://dx.doi.org/10.1016/j.ymssp.2015.09.043

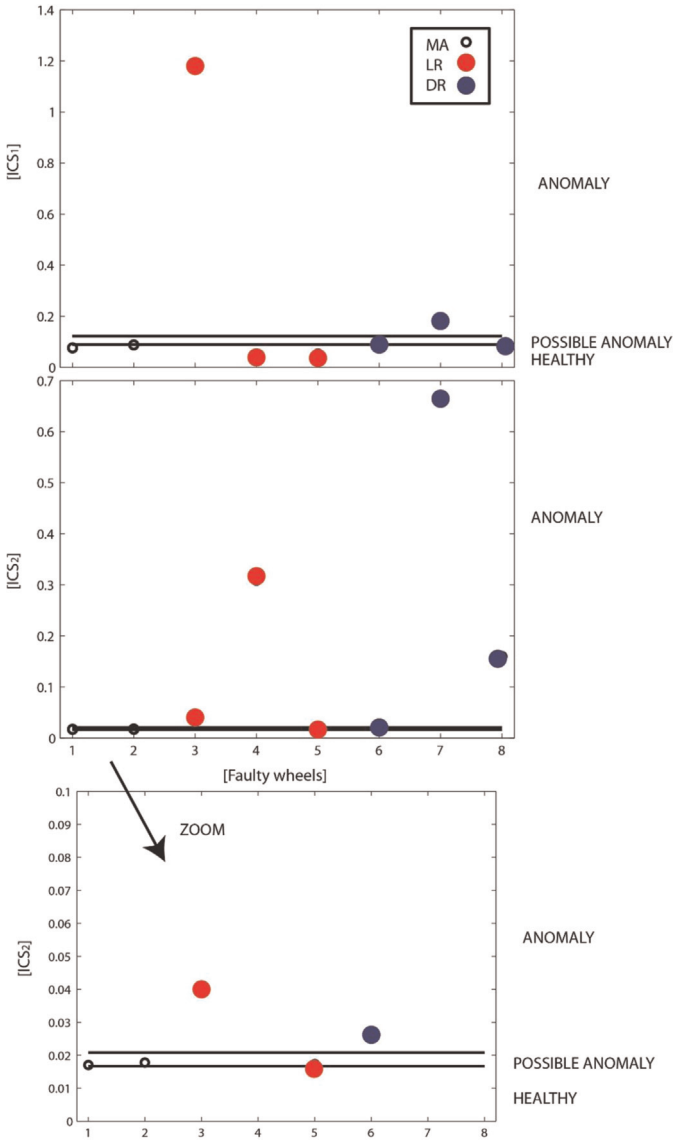

Fig. 25. $\hat{C}^{\alpha}_{1x}$ and $\hat{C}^{\alpha}_{2x}$ pass-fail distributions in case of MA, LR and DR defects.

evaluated and statistical parameters for fault detection (e.g. Kurtosis and RMS) have been used. Furthermore, the cyclostationary nature of the signal has been investigated through the first and second order cumulants and relative indicators.

A non statistical approach (Tukey's method) has been used in order to calculate threshold values for the healthy/faulty discrimination. This activity has enabled the following conclusions to be drawn:

1. The synchronous average and the first order cyclostationarity characterize the deterministic behavior of a system which is usually linked with macro-phenomena that perfectly repeat themselves on a cyclic basis: in case of really localized missing adherence defect (MA) or rust (LR and DR) these techniques are partially efficient since the contact stiffness variations are weakly deterministic;
2. The second-order cyclostationarity characterizes the random behavior of a system: this technique is able to detect all the tested faulty wheels due to the fact that contact stiffness variations are highly non-deterministic;
3. parameter ICS_{2x}, which quantifies the presence of second-order cyclostationary components within the signal, represents a very useful indicators of tread/hub connection anomalies both for missing glue and rust (Fig. 25). Thus, ICS_{2x} can be considered as the key parameter to be adopted in a monitoring test station at the end of the production line.

Please cite this article as: M. Malago', et al., Fault detection in heavy duty wheels by advanced vibration processing techniques and lumped parameter modeling, Mech. Syst. Signal Process. (2015), http://dx.doi.org/10.1016/j.ymssp.2015.09.043

Considering the presented research activity, the main original contributions concern the application of advanced vibration processing techniques to monitoring of heavy-duty wheels and the assessment of their effectiveness, supported by the explanation of vibration sources and characteristics through a simplified lumped parameter model.

References

[1] S. Delvecchio, G. D'Elia, E. Mucchi, G. Dalpiaz, Advanced signal processing tools for the vibratory surveillance of assembly faults in diesel engine cold tests, J. Vib. Acoust. ASME 132 (2) .
[2] G. Dalpiaz, A. Rivola, Condition monitoring and diagnostics in automatic machines: comparison of vibration analysis techniques, Mech. Syst. Signal. Process. 11 (1) (1997) 53–73.
[3] J. Antoni, Cyclic spectral analysis in practice, Mech. Syst. Signal. Process. 23 (2007) 597–630.
[4] J. Antoni, Cyclostationary by examples, Mech. Syst. Signal. Process. 23 (2009) 987–1036.
[5] J. Antoni, R.B. Randall, Rolling element bearing diagnostics - a tutorial, Mech. Syst. Signal. Process. 25 (2011) 485–520.
[6] S. Braun, The synchronous (time domain) average revisited, Mech. Syst. Signal. Process. 25 (4) (2011) 1087–1102.
[7] F. Combet, L. Gelman, An authomated methodology for performing time synchronous averaging of a gearbox without speed sensor, Mech. Syst. Signal. Process. 21 (2007) 2590–2606.
[8] P.D. McFadden, M.M. Toozhy, Application of Synchronous Averaging to vibration monitoring of rolling element bearings, Mech. Syst. Signal. Process. 14 (6) (2000) 891–906.
[9] J. Wismer Time Domain Averaging Combined Order Track. 2012.
[10] K.R. Fyfe, D.S. Munck, Analysis of computed order tracking, Mech. Syst. Signal. Process. 11 (2) (1997) 187–205.
[11] E. Mucchi, A. Vecchio, Acoustical signature analysis of a helicopter cabin in steady-state and run up operational conditions, Measurements 43 (2010) 283–293.
[13] J. Tukey, Exploratory Data Analysis, Addison Wesley, London, UK, 1977.
[14] A. Rivola, E. Mucchi, G. Dalpiaz, Dynamic behavior of gear pumps: effect of variations in operational and design parameters, Meccanica 46 (6) (2011) 1991. 1212.
[15] A. Mikkola, J. Sopanen, Dynamic model of a deep-groove ball bearing including localized and distributed defects Part. 1: Theory, J. Multi-Body Dyn. 217 (2003) 201–211.
[16] A. Mikkola, J. Sopanen, Dynamic model of a deep-groove ball bearing including localized and distributed defects. Part 2: Implementation and results, J. Multi-Body Dyn. 217 (2003) 213–223.
[17] N. Sawhali, R.B. Randall, Simulating gear and bearing interactions in the presence of faults Part. I. The combined gear bearing dynamic model and simulation of localized bearing faults, Mech. Syst. Signal. Process. 22 (2008) 1924–1951.
[18] N. Sawhali, R.B. Randall, Simulating gear and bearing interactions in the presence of faults Part. II. Simulation of of the vibrations produced by extended bearing faults, Mech. Syst. Signal. Process. 22 (2008) 1952–1966.
[19] D.S. Stutts, C.M. Krousgrill, W. Soedel, Parametric excitation of tire wheel assemblies by a stiffness non uniformity, J. Sound. Vib. 179 (3) (1995) 499–512.
[20] D.S. Stutts, W. Soedel, A simplified dynamic model of the effect of internal damping on the rolling resistance in pneumatic tires, J. Sound. Vib. 155 (1991) 153–164.
[21] H. De Gersem, D. Moens, W. Desmet, D. Vandepitte, Dynamic interval analysis of FE models with uncertain substructures, Proc. ISMA 2006 (2006) 4077–4088.
[22] M. Brinkmeier, U. Nackernhorst, S. Petersen, O. Von Estorff, A finite element approach for the simulation of tire rolling noise, J. Sound. Vib. 309 (2008) 20–39.
[23] Werner Schiehlen, Nils Guse, Robert Seifried, Multibody dynamics in computational mechanics and engineering applications, Comput. Methods Appl. Mech. Eng. 195 (2012) 5509–5522.
[24] Jan Helsen, Frederik Vanhollebeke, Ben Marrant, Dirk Vandepitte, Wim Desmet, Multlibody modelling of varying complexity for modal behavior analysis of wind turbine gearboxes, Renew. Energy 36 (2011) 3098–3113.
[25] D. Mba B. Eftekharnejad. Seeded fault detection on helical gears using acoustic emission, in: Proceedings of the 21th International Congress and Exhibition 2008 167 175.
[26] D. Mba M. Elforjani Acoustic emission and natural degradation of a slow speed bearing, in: Proceedings of the 4th World Congress on Engineering Asset Management (WCEAM 2009) 2009 28 30.September.
[27] M.Malago', E.Mucchi, G.Dalpiaz, Condition monitoring and diagnostics in heavy-duty wheels: a first experimental approach, in: Proceedings of the ASME, International Design Engineering Technical Conferences & Computers and Information in Engineering Conference, IDETC/CIE 2009, August 30-September 2, 2009, San Diego, California, USA.
[28] W.A. Gardner, The cumulant theory of cyclostationary time-series, Part I : Foundation, IEEE Trans. Signal. Process. 42 (12) (1994) 3387–3409.
[29] W.A. Gardner, The cumulant theory of cyclostationary time-series, Part II : Development and Applications, IEEE Trans. Signal. Process. 42 (12) (1994) 3409–3429. Giannakis.
[30] C. Capdessus, M. Sidahmed, J.L. Lacoume, Cyclostationary processes: application in gear faults early diagnosis, Mech. Syst. Signal. Process. 14 (3) (2000) 371–385.

Please cite this article as: M. Malago', et al., Fault detection in heavy duty wheels by advanced vibration processing techniques and lumped parameter modeling, Mech. Syst. Signal Process. (2015), http://dx.doi.org/10.1016/j.ymssp.2015.09.043